Parametric Modeling with Beamspread Compensation and MIMO Frequency Domain Inversion Applied to Fine Saturated Sands

Steve Vandenplas, Abdellatif Bey Temsamani, Mikaya L. D. Lumori, *Member, IEEE*, Zobeida Cisneros, and Leo Van Biesen, *Senior Member, IEEE*

Abstract—A system identification technique is applied to estimate the intrinsic absorption and dispersion of two fine sands. The method is based on the parametric modeling of the wave propagation through a Plexiglas tank filled with the sediment under investigation. The applicability of various porous models is discussed. The viscoelastic constant Q model and viscoelastic rational form model are applied and compared. Closed form expressions describing the wave propagation are replaced by Debye series expansions with correction coefficients that consider the beamspread caused by the finite aperture of the emitter. A multiple input multiple output (MIMO) representation is used in conjunction with the maximum likelihood estimator (MLE) for the estimation of the sediment parameters. The estimated absorption and dispersion curves are depicted.

I. Introduction

Within the framework of determining the characteristics of sediments on an acoustic base, a frequency domain system identification technique is used for the parametric modeling of the ultrasonic wave propagation through sediments. An accurate determination of acoustical parameters for sediments is very useful to study the functional relationships between acoustical and geophysical properties. The estimation of the geo-acoustical parameters depends strongly on the validity and accuracy of the models used for wave propagation. The importance of geo-acoustical models in support of acoustic measurements has been emphasized by Hamilton, who has also developed a large number of empirical relationships between various properties of marine sediments [1]–[3]. Bowles [4] has more recently presented a compilation of published measurements of velocity and attenuation as tables and graphs for fine-grained sediments. He argues that, because of a lack of information about the sediment properties, comparison of results remains difficult, and trends that do not always agree with accepted methods for estimating sediment parameters are revealed. Also, the intricacy of the seafloor as an acoustical system makes it difficult to fully accomplish the identification of the sediment's characteristics. Any macroscopic model for the sediment that would attempt to describe fully all microscopic dissipation mechanisms, which stem from many sources, would be extremely complex and of a very limited scope [5].

In this paper, acoustical parameters of two fine sands will be determined in controlled laboratory circumstances. Laboratory measurements allow us to test inverse procedures and validate propagation models. The paper is organized as follows. In Section II, the experimental setup, the measurements and the calibration methods are described. In Section III, the plane wave modeling is described, followed by the beamspread correction with an experimental validation of the correction in Section IV. The inverse procedure is briefly presented in Section V. The parameter estimation results are shown in Section VI. Finally, conclusions are drawn in Section VII.

II. Experimental Setup, Measurements, and Calibration Procedure

The measurement setup consists of a water-filled tank in which a smaller Plexiglas tank containing a known sediment is placed. Before the sediment is put into the water tank, the air content in the sediment is reduced greatly by slowly stirring the sediment in its preparation phase when the particles are mixed with the water. The mixture is then pulled into the Plexiglas container and placed in the water tank in such a way that the grains themselves are not exposed anymore to air. This provides a Plexiglas-sediment-Plexiglas configuration, which is used in conjunction with broadband Panametrics V389 transducers and a pulser-receiver for the transmission experiment Fig. 1. A well-sorted fine sand, "ga38," and a very well-sorted finer sand, "ga39," are used as sediments. Properties of the two sediments are listed in Table I. The transducers are aligned parallel to the Plexiglas surfaces. The thickness of the Plexiglas borders and the sediment layer are 1 and 2 cm, respectively. The emitter-transducer vibrates at a central frequency of 500 kHz. The measured generated pulse and the transmitted or reflected time signal (50 periods) are digitized with a sampling frequency of 10 MHz. Fig. 2 depicts the transmitted and reflected signals for sediment ga39.

Because the inverse problem is based on a frequency domain MLE, the measurement setup is also described in the frequency domain. The elements of the measurement

Manuscript received May 3, 2000; accepted January 12, 2001. This work was sponsored by the EC-MAST-III SIGMA project (No. MAS3-CT97-0100).

S. Vandenplas, A. B. Temsamani, Z. Cisneros, and L. Van Biesen are with the Department of ELEC, Vrije Universiteit Brussel, B-1050, Belgium (e-mail: jsvdplas@vub.ac.be).

M.L.D. Lumori is with the Department of Engineering-L229, University of San Diego, San Diego, CA 92110.

0885–3010/$10.00 © 2001 IEEE

TABLE I
SEDIMENT PROPERTIES.

Sediment Properties	ga38	ga39
Wet bulk density, kg/m^3	1853 ± 10	1855 ± 10
Grain density, kg/m^3	2600	2650
SiO2, %	98.8	> 99.1
Grain size (mean), 10^{-6} m	90	77
	well sorted	very well sorted
Specific surface, cm^2/g	240	325
Apparent specific gravity	1.5	1.5

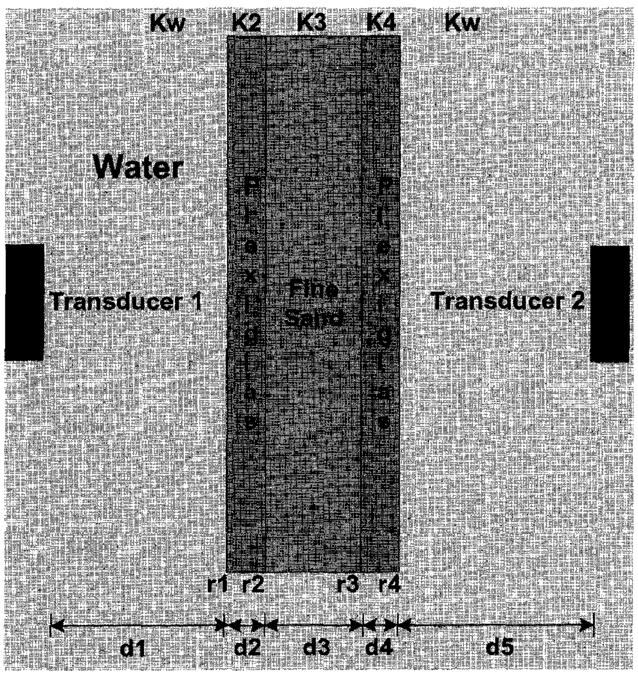

Fig. 1. Experimental setup.

circuits are described by the transfer function, $H_v^{sys}(\omega)$, where subscript v stands for the transmission or reflection experiment. The Fourier transforms of the generated electrical pulse and the transmitted or reflected signal are denoted as $X_v^m(\omega)$ and $Y_v^m(\omega)$, respectively. The relationships between the output and input for the system under investigation are then

$$Y_v^m(\omega) = H_v^{sys}(\omega) H_v^{mea}(\omega, \mathbf{P}) X_v^m(\omega) \tag{1}$$

with $H_v^{mea}(\omega, \mathbf{P})$, the transfer function, describing the wave propagation phenomenon, depending on the parameter vector $\mathbf{P}$, which is to be determined by the inverse procedure. The calibration technique consists of carrying out another experiment under the same conditions with unchanged settings to eliminate $H_v^{sys}(\omega)$. The Fourier transform of the generated electrical pulse and the transmitted or reflected signal are now denoted as $X_v^c(\omega)$ and $Y_v^c(\omega)$.

A similar relationship as (1) can be written for the calibration experiment, viz:

$$Y_v^c(\omega) = H_v^{sys}(\omega) H_v^{cal}(\omega, \mathbf{P}) X_v^c(\omega) \tag{2}$$

with $H_v^{cal}(\omega, \mathbf{P})$, the transfer function, describing the wave propagation phenomenon for the calibration experiment. For transmission, the used calibration consists of performing a pitch-catch experiment in the water tank without the Plexiglas structure. Two calibration methods are possible for the reflection experiment. The first method consists of performing a reflection experiment on an interface with a known reflection coefficient (e.g., water-air interface). In the second method, if the first reflection can be extracted from the rest of the reflections, then this first signal may be used for calibration. In this paper, the second method is adopted, because its calibration and experimental environments are identical. We now define $H_v^m(\omega)$ and $H_v^c(\omega)$ as follows:

$$H_v^m(\omega) = \frac{Y_v^m(\omega)}{X_v^m(\omega)} \quad \text{and} \quad H_v^c(\omega) = \frac{Y_v^c(\omega)}{X_v^c(\omega)}. \tag{3}$$

In fact, $H_v^c(\omega)$ and $H_v^m(\omega)$ can be regarded as the input and output of a single input single output (SISO) system (Fig. 3), whose transfer function, $H_v(\omega, \mathbf{P})$ is

$$H_v(\omega, \mathbf{P}) = \frac{H_v^m(\omega, \mathbf{P})}{H_v^c(\omega, \mathbf{P})}. \tag{4}$$

The elements of the measurement circuit are eliminated in this transfer function, which represents the calibrated wave propagation phenomena and will be modeled parametrically in the next sections.

The Plexiglas parameters were estimated by the MIMO method in this paper. To do this, an extra transmission experiment involving the Plexiglas tank (Plexiglas-water-Plexiglas configuration) is carried out. To simplify the procedure, the multiple reflections of the signals in the water within the Plexiglas container were excluded by windowing. A pitch-catch measurement serves as calibration. The original equations remain valid.

In what follows, the letters T, R and P, in conjunction with subscript v, represent the transmission through sediment-filled Plexiglas tank, the reflection from

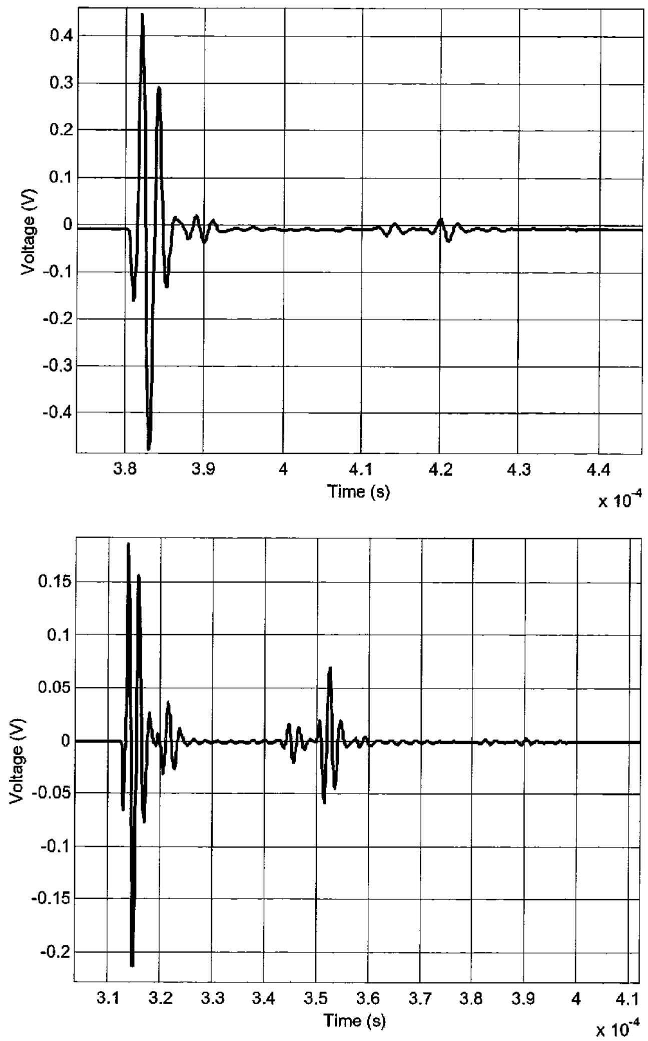

Fig. 2. Transmitted (top) and reflected (bottom) signal for Plexiglas structure filled with sediment ga39.

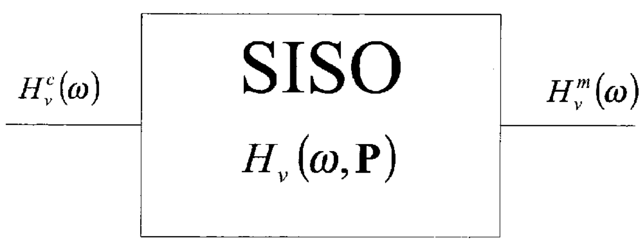

Fig. 3. The SISO system.

the sediment-filled Plexiglas tank, and the transmission through the water-filled Plexiglas tank, respectively. This is summarized in a MIMO context as follows:

$$\begin{bmatrix} H_T^m(\omega) \\ H_R^m(\omega) \\ H_P^m(\omega) \end{bmatrix} = \begin{bmatrix} H_T(\omega,\mathbf{P}) & 0 & 0 \\ 0 & H_R(\omega,\mathbf{P}) & 0 \\ 0 & 0 & H_P(\omega,\mathbf{P}) \end{bmatrix} \begin{bmatrix} H_T^c(\omega) \\ H_R^c(\omega) \\ H_P^c(\omega) \end{bmatrix}. \tag{5}$$

III. Plane Wave Modeling of the Transmission and Reflection Experiment

When modeling the wave propagation through porous materials and considering that the associated wavelength is much larger than the dimensions of the heterogenities (surficial and volumetric), two different main methods are available. The first method assumes that the porous medium can be considered as an isotropic homogeneous medium. Thus, the different dissipation mechanisms involved in the propagation process are indistinguishable in the modeling process. The average dissipation on a representative volume of fluid and solid is considered from a macroscopic point of view. The sediment can be considered as a fluid or as an elastic or viscoelastic solid. Because viscoelastic models are well suited for the description of a broad class of dissipation processes [2], a viscoelastic model for the sediment is used. The stress-strain relationship for the one-dimensional movement is expressed by the generalized law of Hooke [5], [6]:

$$\sigma(\omega) = M(\omega)\varepsilon(\omega) \tag{6}$$

where $\sigma(\omega)$ and $\varepsilon(\omega)$ are the Fourier transforms of the stress and strain, respectively, and $M(\omega)$ stands for the complex modulus.

The Plexiglas-sediment-Plexiglas configuration can then be regarded as a linear viscoelastic multilayer medium. A longitudinal plane wave with a complex wavenumber K_i is then considered to propagate through layer i, viz [6]:

$$K_i = \omega\left(\frac{\rho_i}{M_i(\omega)}\right)^{1/2} = \frac{\omega}{V_i(\omega)} = \frac{\omega}{c_i(\omega)} - j\alpha_i(\omega) \tag{7}$$

where ρ_i is the density, $V_i(\omega)$ is the complex velocity, and $c_i(\omega)$ and $\alpha_i(\omega)$ are the longitudinal dispersion and absorption, respectively. Note that, in Fig. 1, the properties for layers 2 and 4 are identical.

In this paper, the use of a rational transfer function is proposed to model the viscoelastic modulus of the bulk sands. The viscoelastic rational form model has been validated for the wave propagation through Plexiglas [7] and used successfully for describing the behavior of quasi-linear homogenous isotropic viscoelastic composites [6]. Furthermore, in [8], the model has been applied successfully to a silt-clay sample, but no satisfactory results could be obtained for a sand sample.

For the rational viscoelastic model, the complex dilatational phase velocity through layer i is then given by [7]

$$V_i(\omega) = c_i \cdot \sqrt{\frac{1+\sum_{l=1}^{N}\alpha_{i,l}(j\omega)^l}{1+\sum_{k=1}^{D}\beta_{i,k}(j\omega)^k}} = c_i P_i(\omega, \alpha_{i,l}, \beta_{i,k}) \tag{8}$$

where c_i is the frequency-independent phase velocity and $P_i(\omega, \alpha_{i,l}, \beta_{i,k})$ is a function describing the frequency dependence of the complex velocity $V_i(\omega)$. N and D determine the order of the numerator and denominator, respectively. Order (N = 2, D = 1) is found to be optimal when describing the absorption and dispersion of the Plexiglas borders versus frequency [7]. For the sediment, the viscoelastic rational form model will be compared with the more commonly used constant **Q** viscoelastic model [9], where a particular form of the complex modulus $M(\omega)$ is used, leading to a **Q** that is independent of frequency. The complex velocity, $V_3(\omega)$, in the sediment (Fig. 1) is now given by

$$V_3(\omega) = V_{03}\left|\frac{j\omega}{\omega_0}\right|^{\gamma 3} = V_{03}P_3(\omega, \omega_0, \gamma_3) \quad \text{and } \gamma_3 = \frac{1}{\pi}\operatorname{atan}\left(\frac{1}{Q_3}\right) \tag{9}$$

where V_{03} is the frequency-independent velocity for the sediment at a reference angular frequency ω_0.

Observe that the plane wave displacement reflection coefficients r_i and transmission coefficients t_i become slightly frequency dependent, viz:

$$r_i = \frac{P_i(\omega) - Z_{i,i+1}P_{i+1}(\omega)}{P_i(\omega) + Z_{i,i+1}(\omega)P_{i+1}(\omega)} \tag{10}$$

and

$$t_i^2 + 1 = r_i^2. \tag{11}$$

The parameter $Z_{i,i+1}$ is defined as the ratio of the real acoustic impedance Z_{i+1} of layer $(i+1)$ to the real acoustic impedance Z_i of layer (i):

$$Z_{i,i+1} = \frac{Z_{i+1}}{Z_i} = \frac{\rho_{i+1}c_{i+1}}{\rho_i c_i}. \tag{12}$$

By expressing the boundary conditions of the displacement and the stress field, closed form expressions for the transmission and reflection coefficient can be obtained for the calibrated transmission H_T and reflection coefficient H_R [6]–[8]:

$$H_T(\omega, \mathbf{P}) = \frac{N_T(\omega, \mathbf{P})}{D(\omega, \mathbf{P})} \text{ and } H_R(\omega, \mathbf{P}) = \frac{N_R(\omega, \mathbf{P})}{D(\omega, \mathbf{P})} \tag{13}$$

where

$$N_T(\omega, \mathbf{P}) = t_1t_2t_3t_4e^{j\omega\tau_t}e^{-jK_2d_2}e^{-jK_3d_3}e^{-jK_4d_4} \tag{14}$$

and

$$N_R(\omega, \mathbf{P}) = \frac{1}{r_1}\left(r_1 + r_2e^{-2jK_2d_2}\right)\left(1 + r_3r_4e^{-2jK_4d_4}\right) + \frac{1}{r_1}\left(r_1r_2 + e^{-2jK_2d_2}\right)\left(r_3 + r_4e^{-2jK_4d_4}\right)e^{-2jK_3d_3}. \tag{15}$$

The common denominator is given by

$$D(\omega, \mathbf{P}) = \left(1 + r_1r_2e^{-2jK_2d_2}\right)\left(1 + r_3r_4e^{-2jK_4d_4}\right) + \left(r_2 + r_1e^{-2jK_2d_2}\right)\left(r_3 + r_4e^{-2jK_4d_4}\right)e^{-2jK_3d_3}. \tag{16}$$

The numerators [$N_R(\omega, \mathbf{P})$ and $N_T(\omega, \mathbf{P})$] and the denominator [$D(\omega, \mathbf{P})$] are functions of the vector $\mathbf{P}$, which contains the model parameters including delay τ_T given by

$$\tau_T = \frac{d_2 + d_3 + d_4}{c_{0w}} \tag{17}$$

where c_{0w} is the dispersionless phase velocity in water.

A completely different method comprises a model based on the mechanics of porous saturated media. The theory of Biot [10], [11] describes the wave propagation in porous media by a set of coupled differential equations, resulting in the prediction that two dilatational and one rotational wave may propagate through the porous medium. Stoll has pioneered in the application of Biot's theory for modeling of a seabed [12] [13]. In the Biot model, a skeletal frame or matrix containing both the solid and fluid is defined, and the global relative movement of the fluid toward the frame is taken into account, leading to a second, slower, highly attenuated dilatational wave with frame and interstitial fluid moving largely out of phase. It has been found that poroelastic material parameters, such as porosity and permeability, can play an important role in wave propagation through sediments. More recently, Badiey [14] gave an evaluation of Biot sound speeds and attenuations for hard and soft sediments with asymptotic high and low frequency limits. The application of Biot's model requires realistic values for 13 or more different parameters. Despite extensive efforts to gather the geotechnical sediment properties and the study of many empirical relations since the 1950s, the determination of some parameters (e.g., bulk moduli) is still difficult. Numerous methods for choosing these parameters have been published [15]–[17], but their accuracy is still discussed regularly (e.g., [18], [19]) because different combinations of parameters can lead to similar effects on the measurable acoustical parameters.

Note that in the studied case in this paper, because of the experimental setup, which was chosen to avoid possible effects of surface roughness, the global movement of the interstitial fluid toward the frame will be quite small. This could also be experimentally seen in [20], where an underestimated permeability was found, which can be physically interpreted as a low fluid motion relative to the skeletal frame. When this global fluid motion is neglected, the Gassmann equations, which are a special case of the Biot model, can be used [5], [17], [18]. Notice that, in this case, the frame bulk and shear modulus still must be determined as frequency-dependent quantities consistent with experimental results. Therefore, is chosen as the first method to model the sand as a homogeneous viscoelastic medium.

IV. Modeling with Beamspread Correction

Real transducers do not produce plane waves. The divergence of the beam from a plane circular piston transducer can be compensated by an analytic expression derived from the Lommel diffraction integral [21]–[22]:

$$D(s,\omega) = 1 - e^{-js}(J_0(s) + jJ_1(s)) \tag{18}$$

where

$$s = \frac{\omega a^2}{Dc}. \tag{19}$$

a is the radius of the piston transducer, D is the distance of the propagation path, and c is the velocity of the medium. J_0 and J_1 are the Bessel functions of the zeroth and first orders. The error caused by the beamspread and the validity of this diffraction correction will be checked first. A Plexiglas plate is placed at a distance (d_0) of 35 cm from the piston transducer. A reflection experiment in normal incidence is carried out. The transfer function of the measured reflected signal, $H_{r0}^m(d_0,\omega)$ can be modeled as

$$H_{r0}(d_0,\omega) = e^{-2j\omega\frac{d_0}{c_{0w}}} D(s_0,\omega) H_{sys} R_{Plate} \tag{20}$$

and

$$s_0 = \frac{\omega a^2}{2d_0 c} \tag{21}$$

where H_{sys} is the transfer function modeling the influence of the system, R_{Plate} is the reflection coefficient of the Plexiglas plate, and $D(s_0,\omega)$ is the beamspread correction factor at distance d_0. Next, the plate is translated toward the transducer at distances d from the transducer surface, and new reflection experiments are carried out at leading to measured transfer functions, $H_r^m(d,\omega)$, modeled as

$$H_r(d,\omega) = e^{-2j\omega\frac{d}{c_{0w}}} D(s,\omega) H_{sys} R_{Plate} \tag{22}$$

where $D(s,\omega)$ is the beamspread correction factor of the plate placed at distance d from the transducer. H_{sys} and R_{plate} disappear in the expression of the ratio of $H_r(s,\omega)$ and $H_{r0}(s_0,\omega)$:

$$\frac{H_r(d,\omega)}{H_{r0}(\omega)} = e^{-2j\omega\left(\frac{d-d_0}{c_{0w}}\right)} \frac{D(s,\omega)}{D(s_0,\omega)}. \tag{23}$$

The function $E_r(d,\omega)$, defined as

$$E_r(d,\omega) = \frac{e^{2j\omega\left(\frac{d-d_0}{c_{0w}}\right)} H_r^m(d,\omega) D(s_0,\omega)}{H_{r0}^m(d_0,\omega) D(s,\omega)}, \tag{24}$$

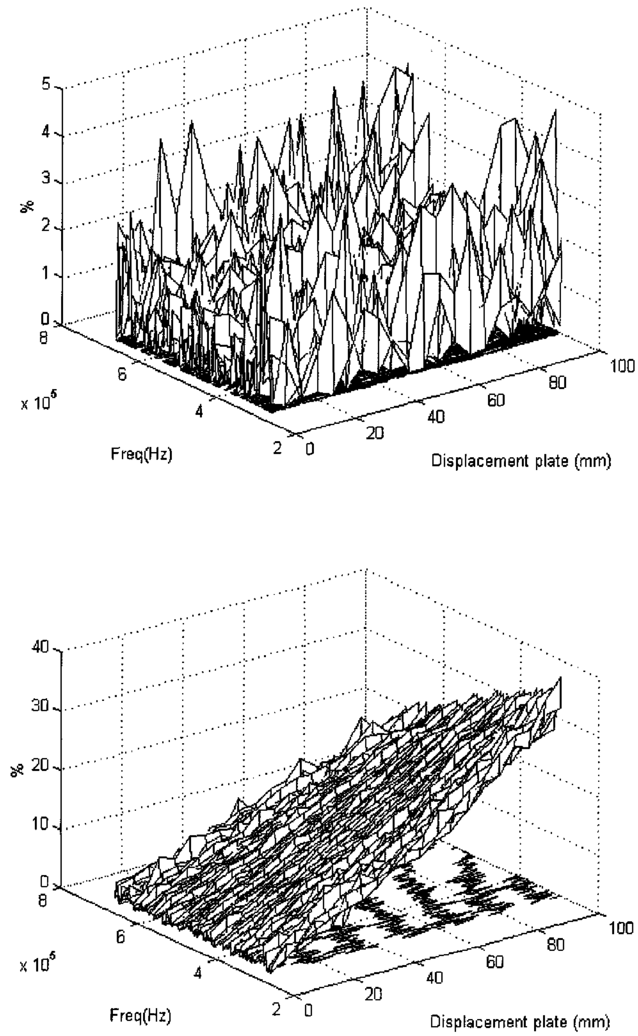

Fig. 4. Relative error in terms of percentage on the amplitude of E_r calculated with beamspread correction factors (top) and with correction factors put to one (bottom).

is equal to 1 in the absence of model errors and noise. Fig. 4(a and b) depicts plots of the relative error, in terms of percentage, on the amplitude of E_r calculated with beamspread correction factors and with the correction factors put to unity, respectively. Relative errors less than 2% are located between 400 and 600 kHz for a 10-cm translation of the Plexiglas. Because of smaller SNR for higher and lower frequencies, the errors rise to 5% for these frequencies. If no beamspread correction is used, errors larger than 30% can be found [Fig. 4(b)] for the lower frequencies, where the divergence effect of the beam is strongest.

As far as the associated phase errors, the errors with beamspread correction are less than 0.5% between 400 and 600 kHz for a 10-cm translation, rising till 0.8% for the higher and lower frequencies.

To introduce the analytic diffraction correction in the reflection and transmission coefficients of the plate, the closed form expression for the plane wave reflection and

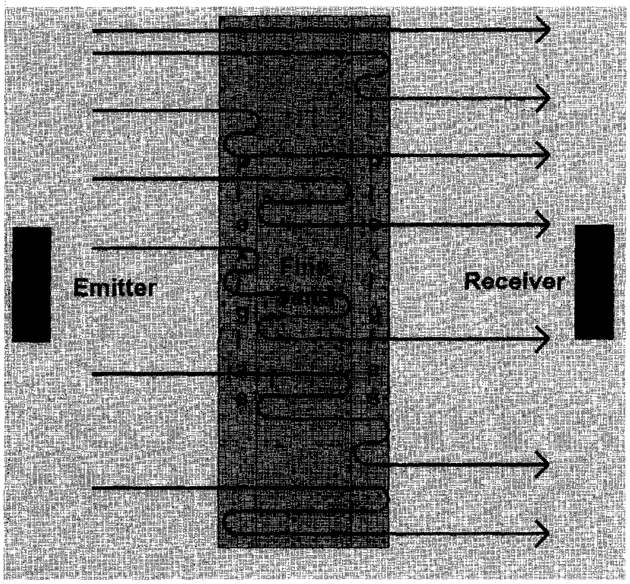

Fig. 5. Dominant propagation paths for transmission through multilayer.

transmission coefficients (13) are replaced by a summation known as the Debye series expansion, corresponding to the multiple propagation paths in the layer [23]. The dominant multiple propagation paths for transmission through the multilayer are shown in Fig. 5.

For each propagation path, the correction for the divergence effect is carried out by multiplying the transmission or reflection coefficient, denoted as T_n and R_n, respectively, for that path, with a beamspread correction coefficient based on the analytic expression given in formula (18). By performing a summation over all propagation paths, the beamspread corrected and calibrated transmission and reflection coefficients are then given, respectively, by

$$H_T(\omega, \mathbf{P}) = \frac{\sum\limits_{n=1}^{\infty} D\left(s_n^T, \omega\right) T_n}{D\left(s_{cal}^T, \omega\right) e^{-j\omega\left(\frac{d_1+d_2+d_3+d_4+d_5}{c_{0w}}\right)}} \text{ and} \tag{25}$$

$$H_R(\omega, \mathbf{P}) = 1 + \frac{\sum\limits_{n=2}^{\infty} D\left(s_n^R, \omega\right) R_n}{D\left(s_{cal}^R, \omega\right) r_1 e^{-j\omega\frac{2d_1}{c_{0w}}}} \tag{26}$$

Parameter s_n^i is now defined with superscript $i = T$ or R, viz:

$$s_n^i = \frac{\omega a^2}{\sum_n^{mult.path} d_n c_n}, \tag{27}$$

and s_{cal}^T and s_{cal}^R are given by

$$s_{cal}^T = \frac{\omega a^2}{(d_1 + d_2 + d_3 + d_4 + d_5)\, c_{0w}} \text{ and} \tag{28}$$

$$s_{cal}^R = \frac{\omega a^2}{2 d_1 c_{0w}}. \tag{29}$$

The summation in (27) is the summation of the products of the distances and velocities over the multiple propagation path. In practice, the infinite summations appearing in (25) and (26) are reduced to finite ones because of the presence of absorption and dispersion in the multilayer and because of the fact that the amplitude of the interface reflection coefficients between two boundaries is smaller than unity. By setting the correction factors equal to unity, the classical plane wave reflection and transmission coefficients are again generated. One can use this property to determine the actual needed number of multiples. A systematic way of achieving this consists of fixing the maximum number of reflections on the interfaces from the multilayer. Even numbers of returns are required for the transmission experiment; odd numbers are needed for the reflection experiment. For the transmission experiment, a maximum of 2, 4, 6, and 8 reflections on interfaces lead to 7, 38, 195, and 988 multiples, respectively. A maximum of 1, 3, 5, and 7 returns on the multilayer conduct to 4, 18, 88, and 441 multiples for the monostatic reflection experiment. The difference in percentage of the amplitudes of summation $\sum\limits_{1}^{\#multiples} T_n$ and $\sum\limits_{1}^{\#multiples} R_n$ with the closed form expression for transmission and reflection through a simulated Plexiglas-sediment-Plexiglas multilayer is shown in Fig. 6. One hundred ninety-five and 88 multiples are chosen for modeling the transmission and the reflection experiment through the filled Plexiglas structure, which implies errors less than 0.05% caused by decomposition in Debye series. By windowing applied to the transmitted signal through the water-filled Plexiglas tank, the Debye series expansion for the corresponding calibrated transmission coefficient can be reduced to a summation of six multiples [see (30), next page], where

$$\tau_P = \frac{2d_2}{c_{0w}} \tag{31}$$

and

$$s_i = \frac{\omega a^2}{(2d_1c_{0w} + 2d_2c_2 + d_3c_3 + d_5c_{0w}) + \sum\limits_{0}^{i} 2id_2c_2} \tag{32}$$

where i = 0, 1, 2.

V. The Inverse Procedure

The estimation of the model parameter vector $\mathbf{P}$ is elaborated using a MLE in the frequency domain. The MLE requires the measurement input and output spectra of the system under investigation as well as knowledge of the perturbing noise variances [24]. The noise sources are assumed to be zero mean, complex normal distributed. This assumption is valid because the measured spectra of the input and output are processed by a discrete Fourier transform [25]. Because the transfer matrix (5) is diagonal by construction, the complexity of the MIMO estimator

$$H_P(\omega, \mathbf{P}) = \frac{\left(1 - r_1^2\right)^2 e^{j\omega\tau_P} e^{-2jK_2d_2} \left(D\left(s_0, \omega\right) + 2D\left(s_1, \omega\right) r_1^2 e^{-2jK_2d_2} + 3D\left(s_2, \omega\right) r_1^4 e^{-4jK_2d_2}\right)}{D\left(s_{cal}^T, \omega\right)} \tag{30}$$

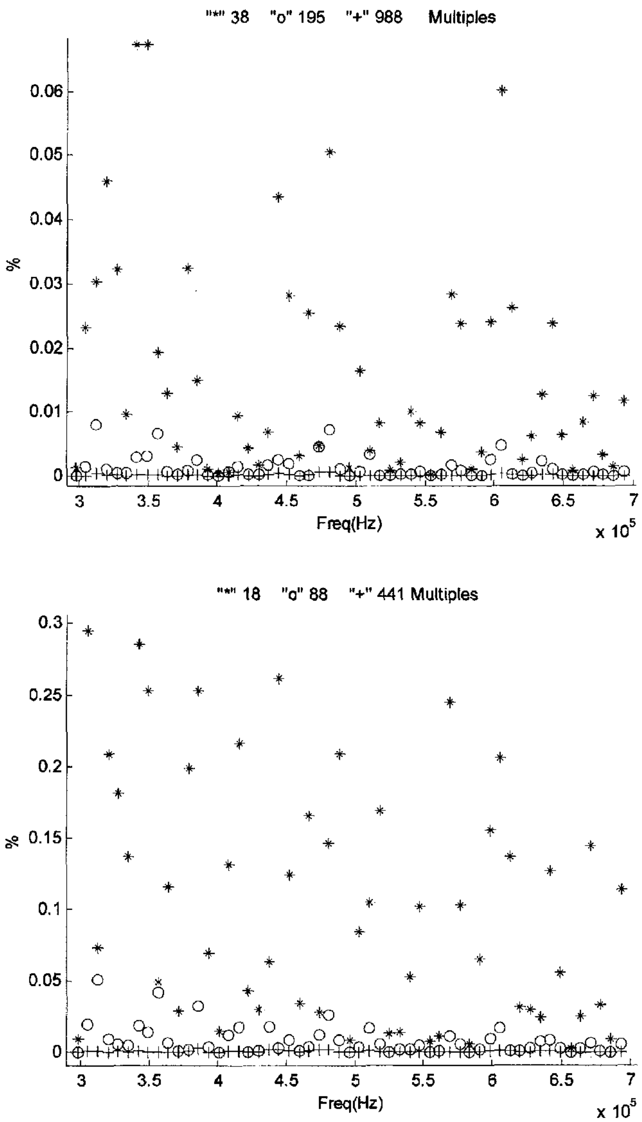

Fig. 6. The difference in percentage of the amplitudes of $\sum_{1}^{\#multiples} T_n$ and $\sum_{1}^{\#multiples} R_n$ with closed form expression for transmission (top) and reflection (bottom) for a simulated rational form (order N = 2, D = 1) Plexiglas-sediment-Plexiglas multilayer. (Used parameters: c_{0w} = 1490 m/s, $c_2 = c_4$ = 2685 m/s, c_3 = 1627 m/s, ρ_1 = 1000 kg/m^3, $\rho_2 = \rho_4$ = 1104 kg/m3, ρ_3 = 1600 kg/m^3, $\alpha_{2,1} = 5.24\mathrm{e}^{-7}$, $\alpha_{2,2} = 4.42\mathrm{e}^{-16}$, $\alpha_{3,1} = 1.38\mathrm{e}^{-6}$, $\alpha_{3,2} = 1.85\mathrm{e}^{-15}$, $\beta_{2,1} = 5.07\mathrm{e}^{-7}$, and $\beta_{3,1} = 1.32\mathrm{e}^{-6}$).

will be reduced. Because of the redundancy of information, the uncertainties on the estimated parameters will be smaller than those obtained with SISO estimators. It is shown in [7] that, by applying the MIMO-estimation method, small model errors could be detected, which were invisible with the SISO method. Furthermore, the MIMO method excludes errors caused by uncertainties on fixed Plexiglas parameters.

Because the generation of acoustical signals is not perfectly synchronized, the $H_{\log}$ technique [26] is used to calculate the averaged signals over the different periods:

$$H_v^k(\omega) = \exp\left(\frac{1}{M}\sum_{i=1}^{M}\log\left(\frac{Y_j^{k,i}(\omega)}{X_j^{k,i}(\omega)}\right)\right) \tag{33}$$

where $k = m, r$ and $v = T, R, P$. The variances on the non-parametric estimates $\sigma^2_{H_v^k}$ are determined during the averaging procedure. The high SNR of the input and output spectra (typically 40 dB) renders the $H_{\log}$ estimates to be almost complex normally distributed, thus satisfying assumptions required by the MLE.

The maximum likelihood cost function to be minimized for the MIMO system is given by

$$\begin{aligned} C_{mimo}(\mathbf{P}) &= C_T(\mathbf{P}) + C_R(\mathbf{P}) + C_P(\mathbf{P}) \\ &= \sum_{l=1}^{L}\left|e_T(\omega_l, \mathbf{P})\right|^2 + \sum_{l=1}^{L}\left|e_R(\omega_l, \mathbf{P})\right|^2 + \\ &\quad \sum_{l=1}^{L}\left|e_P(\omega_l, \mathbf{P})\right|^2 \end{aligned} \tag{34}$$

with

$$e_v(\omega_l, \mathbf{P}) = \frac{H_v^c(\omega_l) H_v(\omega_l, \mathbf{P}) - H_v^m(\omega_l, \mathbf{P})}{\sqrt{V_{e_v}(\omega_l, \mathbf{P})}} \tag{35}$$

and

$$V_{e_v}(\omega_l, \mathbf{P}) = \sigma^2_{H_v^c}(\omega_l)\left|H_v(\omega_l, P)\right|^2 + \sigma^2_{H_v^m}(\omega_l) \tag{36}$$

where $\{\omega_l, l = 1, \ldots, L\}$ denotes the set of angular frequencies to be accounted for. The minimization of (34) toward the parameter vector $\mathbf{P}$ gives rise to a non-linear minimization problem, which is solved with the Levenberg-Marquardt minimization algorithm because of its convergence properties [24].

Initial values for the numerator and denominator coefficients of the rational form for sediments are not available. By starting with a first-order model, selecting a very small parameter, estimating this parameter by minimizing

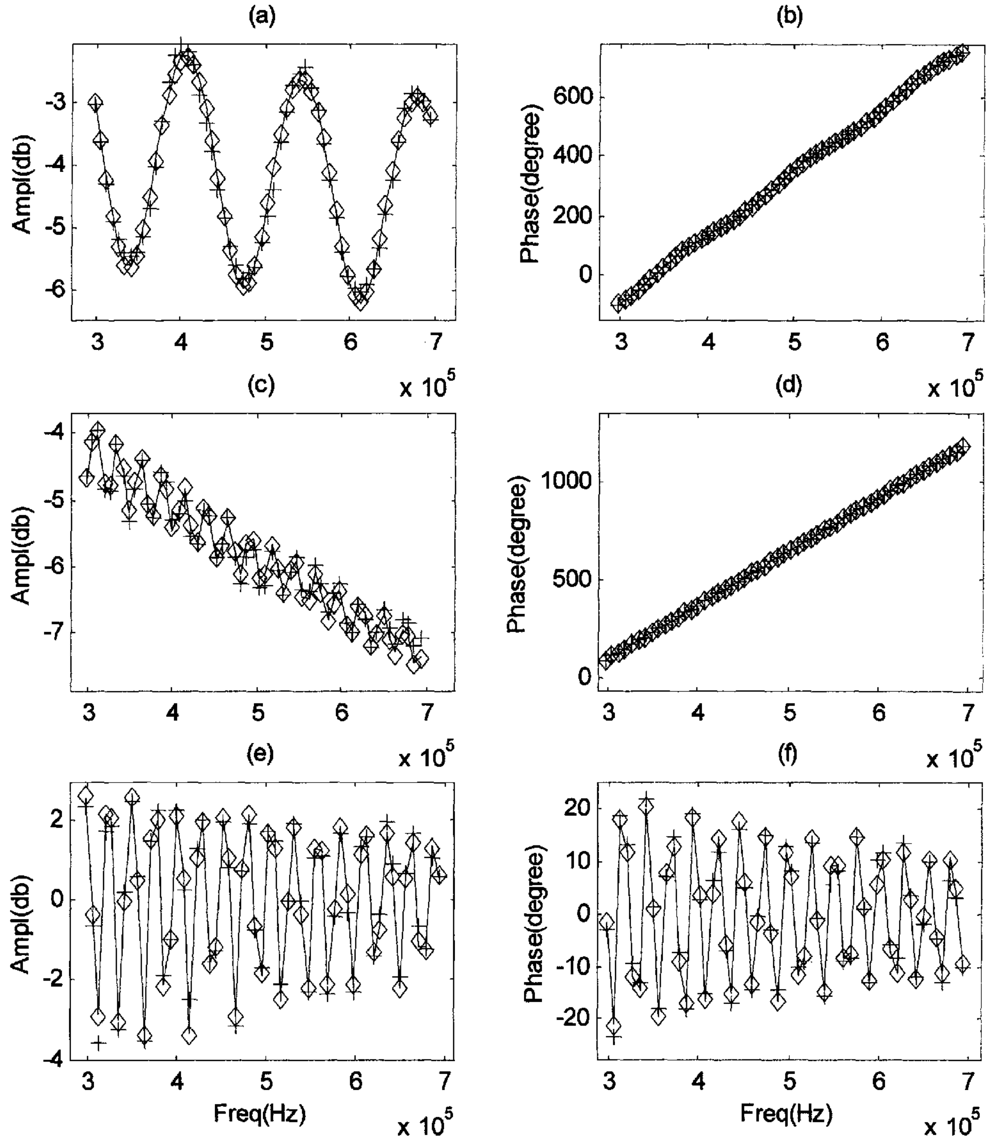

Fig. 7. Results of estimation for sand ga38. Amplitude (a) and phase (b) of calibrated transfer function (TF) through Plexiglas structure without sediment, [(c) and (d)] and filled with sediment [(e) and (f)] TF for reflection: measured TF (+), estimated TF with rational form model (−), and estimated TF with CQ-model (◇).

the cost function, and using the estimated parameter as an initial value for a higher order, the model order can be gradually increased, and initial values can be found. Model order selection for the rational viscoelastic form for the sediments is done on the basis of the decrease in the MIMO cost function (34).

VI. Experimental Results

The results are obtained with the experimental setup presented in Section II (Fig. 1). The used rational form and CQ models for the viscoelastic modeling of the wave propagation of sound through the sediment, with a compensation for the divergence of the beam, are described in Section IV. A system identification approach is adopted to estimate the model parameters of both the sediment and Plexiglas. This was achieved by invoking the MLE in the frequency domain in MIMO sense, as explained in Section V. Order ($\mathrm{N} = 2, \mathrm{D} = 1$) is fixed for the rational transfer function of the Plexiglas. The propagation of multiples in the sediment, the use of the information contained in both the transmitted and the reflected signals, and the calibration method, which is incorporated in the global system identification approach, are assets of the method that are not exploited when carrying out direct measurements of dispersion or absorption with transducers buried in the sediment.

An overview of values for the cost function after minimization toward parameter vector $\mathbf{P}$ is given in Table II. For both sands, a significant decrease of cost function can

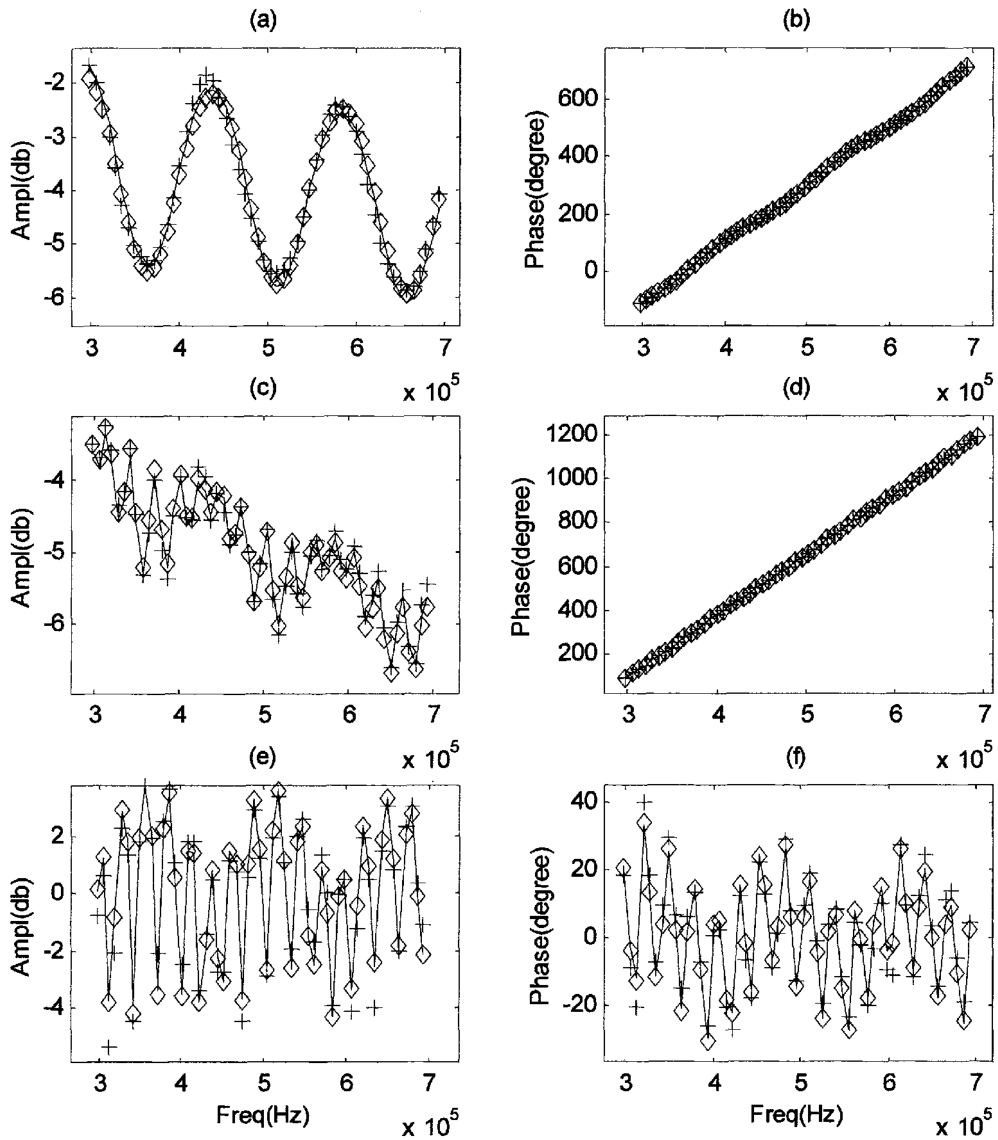

Fig. 8. Results of estimation for sand ga39. Amplitude (a) and phase (b) of calibrated transfer function (TF) through Plexiglas structure without sediment, [(c) and (d)] and filled with sediment, [(e) and (f)] TF for reflection: measured TF (+), estimated TF with rational form model (−), and estimated TF with CQ-model (◇).

TABLE II
OVERVIEW OF OBTAINED COST FUNCTION VALUES.

Model	Viscoelastic rational form model order (1,1)	Viscoelastic rational form model order (2,1)	Viscoelastic rational form model order (2,2)	Viscoelastic Constant Q model
GA38	1.03e5	6.51e4	6.51e4	6.92e4
GA39	1.82e5	1.72e5	1.72e4	1.81e5

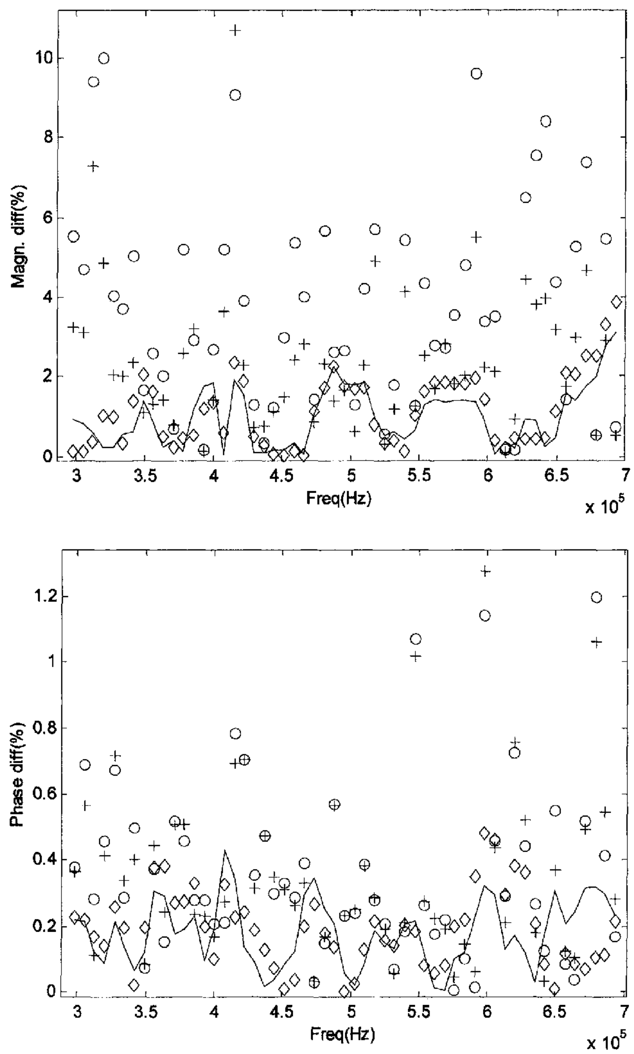

Fig. 9. Amplitude (top) and phase (bottom) differences in terms of percentage between measured and modeled transfer functions for transmission and reflection for Plexiglas structure filled with ga38: transmission from rational form model (−), transmission from CQ-model (⋄), reflection rational form model (∘), and reflection from CQ-model (+).

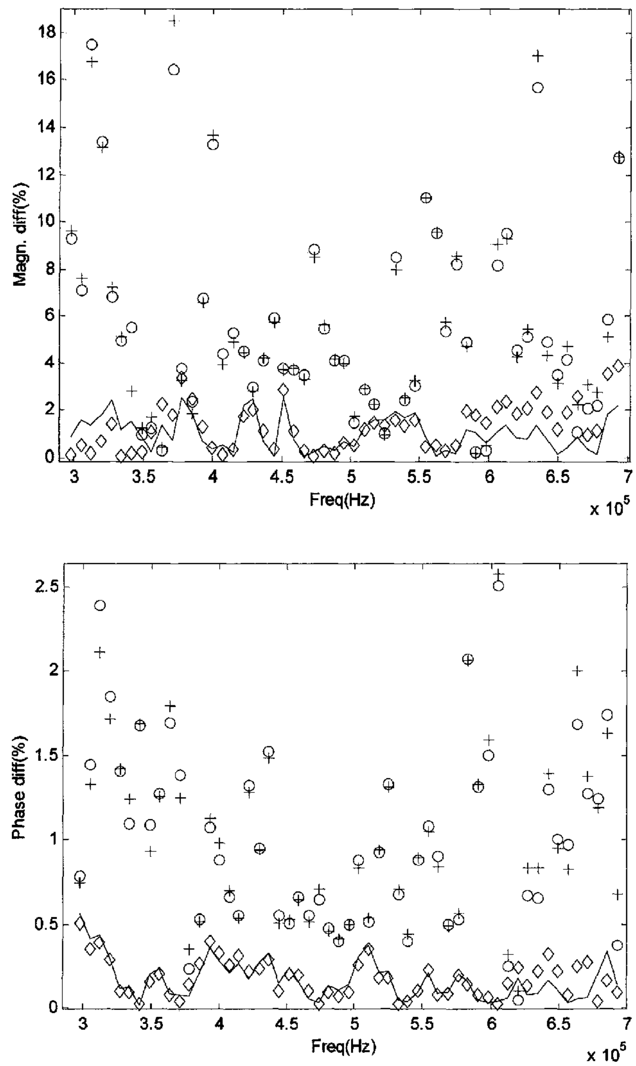

Fig. 10. Amplitude (top) and phase (bottom) differences in terms of percentage between measured and modeled transfer functions for transmission and reflection for Plexiglas structure filled with ga39: transmission from rational form model (−), transmission from CQ-model (⋄), reflection from rational form model (∘), and reflection from CQ-model (+).

be seen by increasing the order from (N = 1, D = 1) to (N = 2, D = 1); a further increase to order (N = 2, D = 2) results only in a slight decrease. It is worth observing that order (N = 2, D = 1) is preferred for the sands. Compared with the values for the cost function when CQ-modeling is used, the rational form model provides a smaller cost function, which is an indication of smaller model errors.

Fig. 7 and 8 show the measured and estimated transfer functions for the Plexiglas structure filled with sands ga38 and ga39, respectively. To shed light on the matter, only one-third of the used 165 spectral lines is presented. Note that the two sediments were contained in two different Plexiglas structures, placed at different distances from transducers. This explains the differences in the shape of the transfer function for transmission through the empty Plexiglas and the differences in the estimated Plexiglas parameters for the two experiments. The differences in percentage between the measured and modeled transfer function for transmission and reflection for the Plexiglas structure filled with ga38 and ga39 can be seen in Fig. 9 and 10, respectively. For transmission, magnitude errors up to 4% in amplitude and 0.5% in phase are readily seen for both sediments of both models. Although the errors for the rational form model and CQ-model are in the same range, bigger differences for the CQ-model are detected. Bigger differences in amplitude and phase can be seen for both models in reflection, especially for ga39.

The estimated model parameters are listed in Table III. Good agreement can be found between the rational form and constant Q estimated densities and velocities. The es-

TABLE III
ESTIMATED PARAMETERS WITH UNCERTAINTY INTERVAL.

Parameter	GA38 viscoelastic rational form model	GA38 viscoelastic Constant Q model ($\omega_0 = 2\pi$ 500 kHz)	GA39 viscoelastic rational form model	GA39 viscoelastic Constant Q model ($\omega_0 = 2\pi$ 500 kHz)
ρ_2 (kg/m^3)	1.630e3 (1e-1)	1.615e3 (1e-1)	1.0635e3 (1e-1)	1.0609e3 (2e-1)
ρ_3 (kg/m^3)	1.8497e3 (3e-1)	1.8472e3 (3e-1)	1.5878e3 (3e-1)	1.5843e3 (3e-1)
c_2 (m/s)	2.67870e3 (8e-2)	2.6738e3 (1e-1)	2.8845e3 (1e-1)	2.8639e3 (2e-1)
c_3 (m/s)	1.65428e3 (9e-2)	—	1.6362e3 (1e-1)	—
V_{03} (m/s)	—	1.67821e3 (2e-2)		1.66186e3 (2e-2)
τ_P (m/s)	1.33096e-5 (1e-10)	1.33094e-5 (1e-10)	1.25648e-5 (1e-10)	1.25645e-5 (1e-10)
τ_T (m/s)	2.68739e-5 (1e-10)	2.68734e-5 (1e-10)	2.653466e-5 (1e-11)	2.653449e-5 (8e-11)
$\alpha_{2,1}$	5.19e-7 (1e-9)	6.34e-7 (2e-9)	4.54e-7 (2e-9)	8.35e-7 (3e-9)
$\alpha_{2,2}$	4.29e-16 (4e-18)	6.39e-16 (4e-18)	5.38e-16 (7e-18)	9.15e-16 (7e-18)
$\alpha_{3,1}$	8.18e-7 (3e-9)	—	1.034e-6 (6e-9)	—
$\alpha_{3,2}$	1.588e-15 (9e-18)	—	9.4e-16 (1e-17)	—
$\beta_{2,1}$	5.02e-7 (1e-9)	6.13e-7 (2e-9)	4.41e-7 (2e-9)	8.04e-7 (3e-9)
$\beta_{3,1}$	7.90e-7 (3e-9)	—	9.98e-7 (5e-9)	—
γ_3	—	5.603e-3 (2e-6)	—	4.073e-3 (2e-6)

timated ga38 densities for both models fall within the uncertainty interval of the measured value listed in Table I. For ga39, however, it seems that the density is underestimated. In the modeling presented here, the density appears only in the interface transmission or reflection coefficients. A possible explanation for this mismatch could be that, for this particular sediment, a transition layer of varying density of non-zero thickness must be taken into account between the Plexiglas and sediment. In the high frequency limit, the wave would only see the step change of density at the interface, but actually not the real bulk density of the sediment underneath [27]. The estimated density must then be considered as a surficial density. Fig. 11 depicts the estimated dispersion and absorption curves calculated with the parameters listed in Table III. Here, very good agreement between the two models for dispersion can be seen. As far as absorption is concerned, an important difference can be seen between the curves for ga39; smaller differences are present for ga38. However, it is worth noting that, at the central frequency of 500 kHz, for which the frequency independent velocity V_{03} was defined, the same value for attenuation is retrieved. Taking into account the lower cost functions and the smaller differences between the measured and the modeled transfer functions for the viscoelastic rational form model, this latter model is preferred for the accurate determination of the dispersion and the absorption curves.

Values of attenuation published in the literature often vary a lot from author to author, because of the type of sediment and because of the utilized measurement method. Moreover the published values of attenuation measured in situ are often values for the total attenuation (the attenuation related to the porous media plus the attenuation associated with the geometry of the subsurface, source, scattering, etc.). Hamilton [1] has reported values measured at 500 kHz for various sands ranging from 90 to

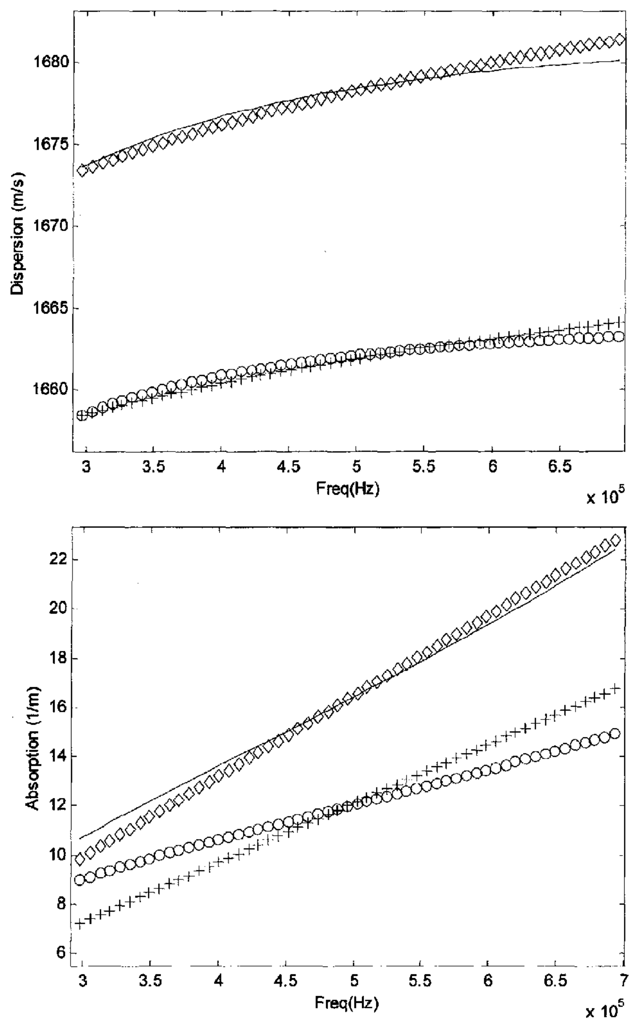

Fig. 11. Estimated dispersion (top) and absorption (bottom) curves: ga38 with rational form model (−), ga38 with CQ-model (⋄), ga39 with rational form model (∘), and ga39 with CQ-model (+).

300 dB/m [att.(dB/m)≈8.686 att. (1/m)]. In the compilation of published values by Bowles [4], at 500 kHz, values of 70 and 90 dB/m were listed for fine-grained sediments. The estimates for the absorption retrieved in this paper are consistent with the broad range of values published in the literature.

VII. Conclusions

In this paper, a global system identification approach was used for an experimental validation of the wave propagation through sediments. A comprehensive motivation for choosing the viscoelastic modeling for the sediment was given. Two viscoelastic models were considered: the viscoelastic rational form and CQ model. A MLE was used to estimate the sediment parameters, and a MIMO representation of a linear system was used to increase the accuracy on the estimated parameters. A beamspread correction was incorporated, and an experimental validation of the correction was elaborated. Good agreement between measured and estimated transfer functions was found for both models. It was shown that using the viscoelastic rational form model, a smaller cost function, compared with the CQ-model, was obtained. Also, good agreement was found between the estimated sediment parameters. The bulk density for one of the sediments was underestimated, which is due to a possible anomaly at the Plexiglas-sediment interface. Estimated absorption and dispersion curves were drawn. These estimation results confirm the validity of the rational form model for describing the wave propagation through sediments, including dispersion and absorption.

References

[1] E. L. Hamilton, "Geoacoustic modeling of the sea floor," *J. Acoust. Soc. Amer.*, vol. 68, no. 5, pp. 1313–1340, 1980.

[2] ——, "Sound velocity and related properties of marine sediments, North Pacific," *J. Geophys. Res.*, vol. 75, no. 23, pp. 4423–4442, 1970.

[3] ——, "Acoustic and other properties of shallow-water sediments off San Diego," *J. Acoust. Soc. Amer.*, vol. 28, no. 1, pp. 1–15, 1956.

[4] F. A. Bowles, "Observations on attenuation and shear-wave velocity in fine-grained, marine sediments," *J. Acoust. Soc. Amer.*, vol. 101, no. 6, pp. 3385–3397, 1997.

[5] T. Bourbié, O. Coussy, and B. Zinszner, "Acoustics of porous media," in *Editions Technip.*. Paris, 1987.

[6] L. Peirlinckx, P. Guillaume, R. Pintelon, and L. Van Biesen, "A global system identification approach for the accurate parametric modeling of ultrasonic reflection and transmission experiments," *IEEE Trans. Ultrason., Ferroelect., Freq. Contr.*, vol. 43, no. 4, pp. 628–639, Jul. 1996.

[7] L. Peirlinckx, R. Pintelon, and L. Van Biesen, "Identification of parametric models for ultrasonic wave propagation in the presence of absorption and dispersion," *IEEE Trans. Ultrason., Ferroelect., Freq. Contr.*, vol. 40, no. 4, pp. 302–312, Jul. 1993.

[8] Z. Cisneros, L. Peirlinckx, and L. Van Biesen, "Parametric modeling and estimation of acoustic sediment properties using a system identification approach," *IEEE Trans. Ultrason., Ferroelect., Freq. Contr.*, vol. 42, no. 6, pp. 1002–1008, Nov. 1995.

[9] E. Kjartansson, "Constant Q-wave propagation and attenuation," *J. Geophys. Res.*, vol. 84, no. B9, pp. 4737–4748, Aug. 1979.

[10] M. A. Biot, "Theory of propagation of elastic waves in a fluid-saturated porous solid, Part I: Low frequency range," *J. Acoust. Soc. Amer.*, vol. 28, pp. 168–178, 1956.

[11] ——, "Theory of propagation of elastic waves in a fluid-saturated porous solid, Part II: High frequency range," *J. Acoust. Soc. Amer.*, vol. 28, no. 2, pp. 179–191, Mar. 1956.

[12] R. D. Stoll, "Theoretical aspects of sound transmission in sediments," *J. Acoust. Soc. Amer.*, vol. 68, no. 5, pp. 1341–1349, Nov. 1980.

[13] ——, "Reflection of acoustic waves at a water-sediment interface," *J. Acoust. Soc. Amer.*, vol. 70, no. 1, pp. 149–156, Jul. 1981.

[14] M. Badiey, "From geology to geoacoustics –Evaluation of Biot-Stoll sound speed and attenuation for shallow water acoustics," *J. Acoust. Soc. Amer.*, vol. 103, no. 1, pp. 309–319, Jan. 1998.

[15] N. P. Chotiros, "Biot model of sound propagation in water-saturated sand," *J. Acoust. Soc. Amer.*, vol. 97, no. 1, pp. 199–214, Jan. 1995.

[16] C. J. Hickey and J. M. Sabatier, "Choosing Biot parameters for modeling water-saturated sand," *J. Acoust. Soc. Amer.*, vol. 102, no. 3, pp. 1480–1484, Sept. 1997.

[17] R. D. Stoll, *Sediment Acoustics*. Berlin: Springer-Verlag, 1989.

[18] ——, "Comments on 'Biot model of sound propagation in water-saturated sand'," *J. Acoust. Soc. Amer.*, vol. 103, no. 5, pp. 2723–2725, May 1998.
[19] N. P. Chotiros, "Response to: Comments on 'Biot model of sound propagation in water-saturated sand'," *J. Acoust. Soc. Amer.*, vol. 103, no. 5, pp. 2726–2729, May 1998.
[20] S. Vandenplas, A. B. Temsamani, Z. Cisneros, and L. Van Biesen, "A frequency domain inversion method applied to propagation models in unconsolidated granular materials," *Ultrasonics*, vol. 38, pp. 195–199, 2000.
[21] P. H. Rogers and A. L. Van Buren, "An exact expression for the Lommel diffraction correction integral," *J. Acoust. Soc. Amer.*, vol. 55, no. 4, Apr. 1974.
[22] A. Bey Temsamani, S. Vandenplas, M.L.D. Lumöri, and L. Van Biesen, "Experimental validation for the diffraction effect in the ultrasonic field of piston transducers and its influence on absorption and dispersion measurements," *IEEE Trans. Ultrason., Ferroelect., Freq. Contr.*, vol. 48, no. 2, pp. 547–559, 2001.
[23] J. Conoir, A. Gérard, and A. Derem, "Ondes acoustiques et séries de Debye généralisées. I. Traitement des interfaces planes," *J. Acoustique*, vol. 4, no. 2, pp. 159–200, Apr. 1991.
[24] J. Schoukens and R. Pintelon, *Identification of linear systems: A practical guideline to accurate modelling.* New York: Pergamon Press, 1991.
[25] R. Pintelon and J. Schoukens, "Robust identification of transfer function in the *s*- and *z*-domains," *IEEE Trans. Instrum. Meas.*, vol. 39, no. 4, pp. 565–573, Aug. 1990.
[26] P. Guillaume, R. Pintelon, and J. Schoukens, "Robust parametric transfer function estimation using complex logarithmic frequency response data," *IEEE Trans. Automat. Contr.*, vol. 40, no. 7, pp. 1180–1190, Jul. 1995.
[27] A. J. Robins, "Reflection of plane acoustic waves from a layer of varying density," *J. Acoust. Soc. Amer.*, vol. 87, no. 4, Apr. 1990.

Steve Vandenplas was born in 1972. He received the degree of ElectroTechnical Engineer (Burgerlijk Ingenieur) in July 1996 from the Vrije Universiteit Brussel (VUB), Belgium. He's currently a PhD research student at the VUB, supported by an IWT fellowship, Department ELEC. His main interests are in underwater acoustics.

Abdellatif Bey Temsamani was born in Tangier, Morocco on March 29, 1973. He graduated with a Bachelor in Applied Sciences in June 1995 from the Abdelmalek Essaadi University, Tetouan, Morocco and received the diploma of Applied Physics directing Computer Sciences (DEA) in June 1996 from the Mons-Hainaut University. He is presently pursuing a Ph.D. in the Electrical Measurement Department at the Vrije Universiteit Brussel (VUB), Brussels, Belgium. His main research interests are ultrasonics, underwater acoustics, and system identification.

Mikaya Lumori (M'89) was born in Yei, Southern Sudan on June 18, 1950. He obtained the B.S.E.E. degree with honors in electronic engineering and the M.S.E.E. in communication engineering in 1971 and 1972, respectively, from UMIST (University of Manchester Institute of Science and Technology) in England. In 1988, he obtained the Ph.D. degree in electrical engineering from the University of Arizona, Tucson. From 1973 to 1977, he was a faculty member (Lecturer) in the Department of Electrical and Electronic Engineering at Makerere University, Kampala in Uganda. In July 1977, he became a founding member of the University of Juba in Southern Sudan, where he worked for several years as Associate Professor and Dean of Students. From 1988 to 1989, he was a faculty research associate at the University of Arizona Health Sciences Center in Tucson. During 1989 to 1990, he was a research scientist with the Medical Research Council Cyclotron Unit, Hammersmith Hospital, London, England. Subsequently, he worked as a research fellow (1990–1991) in the Department of Electrical and Electronic Engineering, University College London, England. In December 1991, he joined the Department of Electrical Engineering, Vrije Universiteit Brussel, in Brussels Belgium (VUB), where he taught courses at Vesalius College (VUB) for over eight years as an associate professor. Since September 2000, Dr. Lumöri has been a tenure-track associate professor of electrical engineering at the University of San Diego, San Diego, CA. His current research interests include Gaussian beam modeling of electromagnetic field sources, applied electromagnetics, electromagnetic hyperthermia, ultrasonics (underwater acoustics and medical applications), and parametric identification in systems.

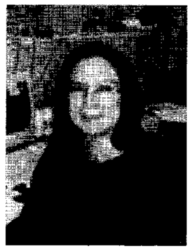

Zobeida Cisneros was born in Guayaquil, Ecuador in 1965. In 1989, she graduated as an engineer in geology at the Escuela Superior Politecnica del Litoral (ESPOL), Guayaquil. Her research pointed to the prospection of gold and groundwater. From 1990 to 1992, and with the support of the Belgian Agency for Cooperation and Development (ABOS), she entered the master's program in fundamental and applied quaternary geology (IFAQ) at the Vrije Universiteit Brussel (VUB). In 1992, she joined as a research fellow (IUAP-20) the Department of ELEC of the Free University of Brussels. In the frame of the modeling of the North Sea, her work points to the relationships between the geomechanics of marine sediments and the acoustic measurements on them.

Leo Van Biesen (M'90–SM'95) was born in Elsene, Belgium, on August 31, 1955. He received the degree of Electro-Mechanical Engineer from the Free University of Brussels (VUB), Brussels in 1978, and the Doctoral degree (Ph.D.) from the same university in 1983. From 1978 to 1982, he received a fellowship from the Belgian Institute for the Encouragement of the Research in Industry and Agriculture (IWONL). During this period, he carried out research on automated cable fault location techniques, which lead to the doctoral degree. This work was done in cooperation with the Belgian Company Balteau. Dr. Van Biesen was awarded the 100th Anniversary Award of the Royal Belgian Society of Electrotechniques in 1984 for doctoral research work.

From 1983 on, he was a senior assistant in the Department of Fundamental Electricity and Instrumentation of the Free University of Brussels. In 1983, he started his career as a lecturer until he was nominated a part-time lecturer. In 1985, he joined the Rectorial Services of the same university to be in charge of the management of the Research and Development Department of the University. He occupied this function until 1987. In 1988, he becomes a full-time lecturer (professor). He teaches courses on fundamental electricity, electrical measurement techniques, signal theory, computer-controlled measurement systems, and telecommunication. He is also the Director of the "Earth Technology Institute" of the Free University of Brussels. His current interests are signal theory, modern spectral estimators, time domain reflectometry, underwater acoustics, and expert systems for intelligent instrumentation.

He has been chairman of IMEKO TC-7 from 1994 to 2000 and is currently President-Elect of the International Measurement Confederation (IMEKO) for the period 2000 to 2009.